

http://pubs.acs.org/journal/aesccq Article

Modeling of the Atmospheric Process of Cyanobacterial Toxins in Algal Aerosol

Victoria Zorbas, Myoseon Jang,* Baharan Emam, and Jiwon Choi



Cite This: ACS Earth Space Chem. 2023, 7, 1141–1150



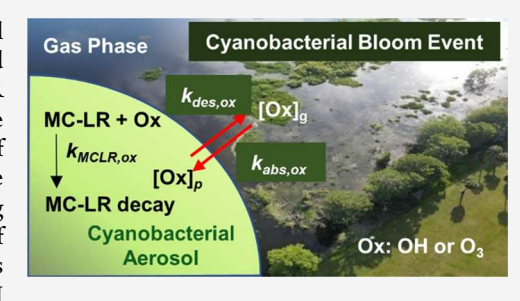
ACCESS I

III Metrics & More

Article Recommendations

Supporting Information

ABSTRACT: The degradation of microcystin-LR (MC-LR) in cyanobacterial aerosol with atmospheric oxidants, such as ozone and OH radicals, was predicted by the Harmful Algal Aerosol Reaction (HAAR) model. The ozonolysis of MC-LR in cyanobacterial aerosol at nighttime and its photooxidation during the daytime was observed in an outdoor chamber. The HAAR model simulates the impact of humidity and aerosol compositions on MC-LR decay. In the model, gas-particle partitioning of atmospheric oxidants onto algal aerosol was kinetically treated using the absorption and desorption processes. In the model simulation, the half-life of MC-LR estimated with its ozonolysis rate constant (3 \times 10 $^{-11}$ cc/molecules/s) is 4.6 h \pm 0.92 at 66 ppb ozone. With the reaction rate constant for MC-LR with OH



radicals $(6 \times 10^{-7} \text{ cc/molecules/s})$, the estimated half-life of MC-LR during daytime under Florida's typical summer sunlight is 6 minutes, suggesting that the reaction with OH radicals dominates daytime MC-LR decay. Under moderate sunlight with a typical wind speed (9.2 km/h), the dispersion and HAAR models predict that 25% of aerosolized MC-LR undergoes the atmospheric process within 0.92 km from a bloom source in Florida's largest lake, suggesting the critical role of the atmospheric oxidation of MC-LR decay.

KEYWORDS: harmful algal blooms, microcystin-LR, cyanobacterial algae, atmospheric oxidation, algal aerosol

1. INTRODUCTION

Over the last decades, research on freshwater algal blooms has uncovered a plethora of toxins produced by cyanobacteria. There is a significant concern that over the next few years, due to climate change, a significant increase in the intensity and frequency of freshwater algal blooms will be observed, exacerbating the negative consequences associated with cyanotoxins. ^{1,2} Algal toxins are considered to threaten humans, animals, and the ecosystem. ³⁻⁷ Recent research has revealed more than 2,300 cases of contaminated lakes in the contiguous United States and more than 5000 in Alaska. ⁸

Among all cyanotoxins, the most notorious ones are the hepatotoxic microcystins (MCs), with over 100 identified congeners. The (all-S,all-E)-3-amino-9-methoxy-2,6,8-trimethyl-10-phenyldeca-4,6-dienoic acid (ADDA) bond is unique in MCs and plays a contributory role in MC binding with other molecules and inhibition of protein phosphatases in mammalian cells. Wang et al. 11 report that chronic, low-dose MC-LR exposure in mice by intratracheal injection induced alveolar collapse and lung cell apoptosis as well as a breach of cell junction integrity.

In addition to ingestion and dermal contact, inhalation is a likely pathway to human exposure to cyanobacterial toxins. Algae cells, bacteria, and waterborne toxins can be incorporated into the atmospheric air via a bubble-bursting process by a wind-driven wave mechanism. ^{12,13} When bubbles formed by trapped air rise to the water surface, they burst and form jet

and film drops. ¹⁴ Organic materials, salts, bacteria, and algae on the water surface are ejected with and transferred into the air by the formation of droplets. ¹³ Many cyanobacterial species, including MCs, have been detected in the aerosol. ^{15,16} Their size fractions are considered respirable, causing multiple adverse effects on human and animal populations onshore. Despite the growing consensus on the health risks for persons living and working near lakes and estuaries contaminated by cyanobacteria, the potential exposure pathway of the inhalation of aerosolized blue-green algae has not yet been understood. ¹⁷

Atmospheric processes can affect the longevity of cyanobacterial toxins in the algal aerosol. Preliminary studies show that the direct photolysis of the MCs in water is insignificant. On the contrary, the aerosolized MCs can be rapidly oxidized by abundant atmospheric oxidants like ozone or OH radicals. Studies suggest that the ADDA unit of MC-LR in a cyanobacterial aerosol can be decayed via heterogeneous chemistry in the aerosol phase. For instance, Jang et al. define the second-order ozonolysis rate constant of MC-LR in cyanobacterial aerosol by using chamber data. To date, no

Received: February 22, 2023
Revised: April 14, 2023
Accepted: April 14, 2023
Published: May 3, 2023





Table 1. Experimental Conditions of Atmospheric Oxidation of MC-LR Performed with Algal Aerosol in the UF-APHOR Chamber

exp.	date	aliquot	UV	[MC-LR] ₀ ^c ppt	[NO] ₀ ppb	[2M2B] ₀ ppb	$\begin{bmatrix} O_3 \end{bmatrix}_0^d$ ppb	$M_{\text{in,dry}_3}^{e} (\mu g/m^3)$	$M_{ m or,dry}/M_{ m in,dry}^{f}$	RH (%)	T (K)	comments
A	5/24/2022	Microcystis aeruginosa	no	1.47	3.4	N.A.	161	85	0.7	36	297-295	Figure 2 and S1
В	5/24/2022	Microcystis aeruginosa	no	0.65	3.2	N.A.	145	68	0.8	95	296-297	Figures 2 and S1
С	4/10/2022	Microcystis aeruginosa	no	3.07	1.5	N.A.	66	46	1.9	89	278-280	Figures 2 and S1
D	4/10/2022	Microcystis aeruginosa ^a	no	2.38	1.5	N.A.	111	44	1.7	49	277-279	Figures 2 and S1
E	4/14/2022	Microcystis aeruginosa	no	2.38	2	N.A.	103	43	1.8	43	292-294	Figures 2 and S1
F	5/4/2022	Microcystis aeruginosa	no	0.77	4.8	N.A.	104	18	2.4	95	291-292	Figures 2 and S1
G	2/11/2022	Anabaena sp. ^b	yes	2.66	54	74.5	2.3	43	1.8	90-30	279-305	Figures 3 and S1
Н	2/11/2022	Anabaena sp.	yes	2.57	280	70	2.2	40	1.7	91-33	280-306	Figures 3 and S1
I	2/20/2022	Anabaena sp.	yes	1.24	37	52.5	4.2	53	0.9	38-11	279-304	Figures 3 and S1
J	2/20/2022	Anabaena sp.	yes	1.67	33	70.7	2	53	1	91-70	279-300	Figures 2 and S1

 a M. aeruginosa BLCC-F108 is a high-MC-producing strain that was isolated from Lake Okeechobee, Florida, during a massive algal bloom in 2019 and cultured at UF/IFAS. b Commercially available Anabaena (=dolichospermum) (VWR International LLC). The MC-LR measured in cyanobacterial aerosol originates mostly from the spiked MC-LR. c For all of the experiments, 25 μ L of MC-LR solution (1 mg of MC-LR to 1 mL of methanol) was added to 5 mL of the green algae aliquot. The unit of MC-LR concentrations is in ppt in the air volume. d Initial concentration of ozone. The ozone concentration increases during the daytime due to the photochemical reaction of hydrocarbons in the presence of NO_x. e The concentration of dry inorganic mass in cyanobacterial aerosol is calculated using ACSM and IC data. In addition, $M_{\text{in,dry}}$ can be determined by using $M_{\text{or,dry}}M_{\text{or,dry}}M_{\text{or,dry}}M_{\text{or,dry}}$ s hygroscopicity, $M_{\text{in,dry}}$'s hygroscopicity (Section 2.2), and $M_{\text{tot,dry}}$ (SMPS and aerosol density) by using an optimizing method. f Organic dry mass to inorganic dry mass ($M_{\text{or,dry}}/M_{\text{in,dry}}$) in an algal aerosol. Water mass is calculated by the hygroscopicity regression curves for inorganic mass and organic mass separately.

model is available to predict the decay of MCs in aerosolized cyanobacterial algae. In order to accurately simulate the atmospheric processes of MCs, the model needs to consider the kinetic rate constants with different oxidants, such as ozone and OH radicals. In addition, aerosol parameters like hygroscopicity and aerosol compositions, which influence the multiphase partitioning of oxidants, need to be incorporated into the model. Therefore, the need for in-depth research on the atmospheric aging of cyanobacterial aerosol acted as a driving force for conducting this study.

The harmful algal aerosol reaction (HAAR) model was developed for the prediction of atmospheric processes of MC-LR, which is the most abundant in nature. A series of experiments were conducted using the Atmospheric PHotochemical Outdoor Reactor located at the University of Florida (UF-APHOR) under controlled environmental conditions (i.e., humidity, temperature, ozone, NOx, hydrocarbon, and sunlight) during nighttime and daytime. The oxidation of MC-LR was considered to occur via heterogeneous reactions with atmospheric oxidants (O₃ and OH) in the aerosol phase. The aerosol water content and the aerosol composition were included in the model as significant parameters that affect the overall process of the MC-LR decay in the cyanobacterial aerosol to accurately simulate the multipartitioning of oxidants. The rate constant between MC-LR and ozone was determined by simulating nighttime chamber data. The resulting ozonolysis rate constant of MC-LR was then applied to daytime simulation to determine the reaction rate constant of MC-LR with the OH radical. The simulated degradation of MC-LR in algal aerosol using the HAAR model was compared to the enzyme-linked immunosorbent assay (ELISA) data of

the algal aerosol that was atmospherically aged under varying conditions in the UF-APHOR chamber.

2. EXPERIMENTAL SECTIONS

2.1. Chamber Experiments. To study the decay of MC-LR under different environmental conditions, the algae culture aliquot (Microcystis aeruginosa or Anabaena sp.) was nebulized into the UF-APHOR dual chambers (52/52 m3) and atmospherically aged in the presence of oxidants (O3 and OH). Both M. aeruginosa and Anabaena sp. are common species of freshwater cyanobacteria on a global scale.^{20,21} The commercially available Anabaena sp. (VWR International LLC, GA) was purchased and cultured in our laboratory for 2 months. M. aeruginosa originating from Lake Okeechobee, which is notorious for harmful algal aerosol blooms, was cultured in the University of Florida's Institute of Food and Agricultural Sciences (UF-IFAS) and provided to our Lab. M. aeruginosa cultures were grown in liquid BG11 medium at 25 °C under a 12:12 h light:dark cycle. 22 Table 1 summarizes experimental chamber conditions. Laboratory culture of the strain of toxic M. aeruginosa was used for experiments A-F (Table 1) and commercially available Anabaena sp. for experiments G-J (Table 1).

A detailed description of the chamber experimental procedure and information on instrumentation and chemical used for this study can be found in Section S1 in the Supporting Information (SI). Briefly, the chamber experiments were conducted at high concentrations of cyanobacterial aerosol to provide aerosols for various chemical analyses. Specifically, cyanobacterial aerosol (40–250 μ g·m⁻³) was oxidized with ozone (60–160 ppb) at nighttime. The algal aerosol containing MC-LR was shortly introduced into the

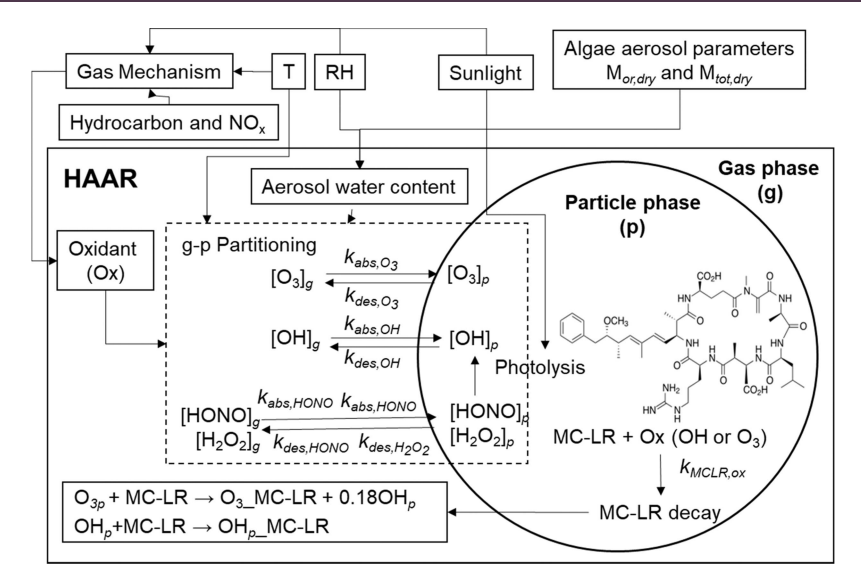


Figure 1. Components of the HAAR model to process the oxidation of MC-LR in an algal aerosol. Subscripts "g" and "p" denote the gas phase and the particle phase, respectively. Gas-particle partitioning of oxidants (ox), such as OH and O₃, is kinetically processed by using the absorption rate constant $(k_{\text{abs,ox}})$ and desorption rate constant $(k_{\text{des,ox}})$. The photolysis of HONO and H₂O₂ in the aqueous phase can also produce OH radicals. $k_{\text{abs,HONO}}$ and $k_{\text{abs,HONO}}$ are the absorption rate constants for HONO and H₂O₂, respectively. $k_{\text{des,HONO}}$ and $k_{\text{des,H₂O₂}}$ are the desorption rate constants of HONO and H₂O₂, respectively. $k_{\text{MCLR,ox}}$ is the reaction rate constant of the oxidation of MC-LR with oxidants (OH and O₃). T and RH are the temperature and relative humidity, respectively. $M_{\text{or,dry}}$ and $M_{\text{tot,dry}}$ are the dry organic mass and the total dry mass $(\mu g \cdot m^{-3})$, respectively.

chamber in the presence of ozone. For daytime oxidation, MC-LR in cyanobacterial algal aerosol was also photochemically aged in the presence of 2-methyl-2-butene (2M2B) (50-80 ppb) and NO_x (30-280 ppb), as seen in Table 1. Figure S1 shows the time profiles of 2M2B, ozone, and NO_x concentrations, and the gas simulation of 2M2B in the presence of NO_x and under ambient sunlight. Figure S2 illustrates the time profile of the sunlight intensity on 02/20/ 2022. For all experiments, 25 μ L of Microcystin-LR (MC-LR, >95%, Cayman Chemical, Ann Arbor, Michigan) solution (1 mg of MC-LR in 1 mL of methanol) was added to 5 mL of the cyanobacterial aliquot solution. The resulting solution was then sonicated for cell lysis and nebulized into the chamber. The geometric mean diameter of the regulating algal aerosol ranged from 65 to 115 nm with geometric standard deviations between 1.65 and 1.95 nm.

A particle-into-liquid sampler (PILS) (Applikon, ADI 2081) was used to collect aerosol within a small amount of water at an airflow rate of 13–14 (L·min⁻¹).^{23–25} The MC-LR concentration in each sample was measured in duplicate using an ELISA kit (Eurofins Analytics, Warminster, PA). All samples were analyzed within 24 hours of sample collection. The concentration of particles in the collected samples was calculated using the gas and liquid flow rates of the PILS, the data from a scanning mobility particle sizer (SMPS, TSI, Model 3080) integrated with a condensation nuclei counter (TSI, Model 3022), and the density of aerosol (1 g·mL⁻¹ approximately).

2.2. Algal Aerosol Hygroscopicity. The water content in algal aerosol was measured by using a Fourier transform infrared (FTIR) spectrometer equipped with a specially fabricated optical flow tube that regulated humidity between 25 and 90%. The intensity of the OH stretching bands (centered at 1650 and 3350 cm⁻¹) increases with increasing humidity. The FTIR intensity of liquid water in wet NaNO₃ particles provided a reference for quantifying the liquid water content of various aerosols on a silicon disk since its

thermodynamic properties are known.^{30,31} Algal aerosol was collected on a silicon disk (13 mm \times 2 mm, Sigma-Aldrich) using a home-built impactor and analyzed using the FTIR spectrometer (Nicolet iS50, Thermo Fisher Inc.) in transmission mode. The FTIR disc was weighed using an analytical balance before and after particle impaction to measure the particle mass. The hygroscopicity measurement experiment was conducted separately in the case of high inorganic and organic contents. To separate hydrogel-like algal organics, the algal aqueous solution was centrifuged (12,000 rpm) for 5 min. The organic enriched portion was located at the bottom of the centrifuge tube. The supernatant that included water-soluble inorganic salts was separated by using a pipette. To further remove inorganics, organics were washed three times with water. These organics were applied to measure the functional group compositions of algal organic matter originating from both M. aeruginosa and Anabaena sp. cultures by using an FTIR spectrometer as well as hygroscopicity of the decoupled organics and inorganics.

3. HAAR MODEL

HAAR is a kinetic model developed to predict the atmospheric processes of MC-LR concerning reactions with different oxidants under various environmental conditions, such as sunlight, humidity, and air pollutants (i.e., NO_x and hydrocarbons). The mixing state between algal organic and inorganic salts is assumed to be a single-homogeneous phase owing to the abundant polar functionality of cyanobacterial constituents. The key model components consist of gas-aerosol partitioning of atmospheric oxidants into liquid-like cyanobacterial aerosol and the kinetic mechanisms of MC-LR with major atmospheric oxidants (O_3, OH) . In addition, parameters, such as the hygroscopicity and the chemical composition of cyanobacterial aerosol, were introduced into the model. The HAAR model, which was built in conjunction with the gas kinetic model in the box model platform was simulated with a kinetic chemical solver under the dynamically simple model of atmospheric

chemical complexity (DSMACC) 31,32 integrated with the kinetic preprocessor (KPP). 33,34 The formation of atmospheric oxidants in the presence of hydrocarbons and NO_x was processed using explicit gas mechanisms, such as the Master Chemical Mechanism (MCM version 3.3.1). 34 The overall schematic of the HAAR model is shown in Figure 1.

3.1. Gas-Particle Partitioning of Oxidants onto Algal Aerosol. The absorption mode governs the gas-aerosol partitioning of atmospheric oxidants onto liquid-like cyanobacterial aerosol. The reaction of MC-LR with oxidants is assumed to occur in the bulk phase based on the small diffusereactive parameter, q, which is estimated by using a rate constant, the diffusion coefficient of the oxidant in liquid media, and the aerosol size. For example, the q value of ozone is in the order of 10^{-3} . The gas-particle partitioning coefficient (K_{p-ox}) of an oxidant (ox) on the algal particle (p) is expressed in eq 1.

$$K_{\rm p_ox} = 0.082TK_{\rm H,ox}V_{\rm tot,aerosol} \tag{1}$$

 $K_{\rm p_ox}$ is unitless expressed in L/L of air. The temperature (T) dependency of $K_{\rm p_ox}$ is derived from Henry's law constant $(K_{\rm H,ox})^{.37,38}$ $V_{\rm tot,aerosol}$ is the total aerosol volume in L/L of air.

The water content of algal aerosol is estimated with the hygroscopicity of both inorganic and organic constituents in aerosol by using FTIR data (Section 2.2). $M_{\rm or,dry}$, $M_{\rm in,dry}$, and $M_{\rm tot,dry}$ are the dry organic mass, the dry inorganic mass, and the total dry mass ($\mu {\rm g \cdot m^{-3}}$), respectively. The resulting regression equations for hygroscopicity (water mass normalized with $M_{\rm or,dry}$ or $M_{\rm in,dry}$) of each component are illustrated in Figure S3. $V_{\rm tot,aerosol}$ is the sum of $M_{\rm tot,dry}$ and the aerosol water content, which is estimated from aerosol hygroscopicity. In general, the aerosol water content increases at higher RH increasing $V_{\rm tot,aerosol}$ and thus, increasing $K_{\rm p_ox}$. In addition, $K_{\rm p_ox}$ for ozone increases with increasing the fraction of $M_{\rm or,dry}$ to $M_{\rm tot,dry}$, as seen in eq 2.

$$K_{\text{p_ox}} = 0.082TK_{\text{H,ox}}V_{\text{tot,aerosol}} \left(1 + \frac{M_{\text{or,dry}}}{M_{\text{tot,dry}}}\right)$$
(2)

The higher the organic fraction in the aerosol, the higher the ozone solubility appears.³⁹ Thus, the degradation of MC-LR is influenced by the concentration of oxidants partitioned onto algal aerosol, and thus it is also impacted by the aerosol composition and the aerosol water content associated with humidity.

In the model, the gas-particle (g-p) partitioning of ox on algal aerosol is kinetically expressed by using the absorption $(k_{\rm abs,ox})$ and desorption $(k_{\rm des,ox})^{40-42}$ rate constants, as represented in eqs 3, and 4.

$$ox_g \rightarrow ox_p \quad k_{abs,ox}(s^{-1})$$
 (3)

$$ox_p \rightarrow ox_g \quad k_{des,ox}(s^{-1})$$
 (4)

 $k_{\rm abs,ox}$ is calculated using eq 5 as follows 41,43

$$k_{\text{abs,ox}} = f_{\text{abs,ox}} M_{\text{tot,aerosol}} \frac{\omega_{\text{ox}} f_{\text{p,mass_to_surface}}}{4}$$
 (5)

where $f_{\rm p,mass_to_surface}~({\rm m}^2\cdot\mu{\rm g}^{-1})$ is the coefficient to convert the aerosol mass concentration ($\mu{\rm g}\cdot{\rm m}^{-3}$) to the surface area concentration (${\rm m}^2\cdot{\rm m}^{-3}$) from particle size distribution. $f_{\rm abs,ox}$ is the coefficient for the uptake process. The total mass aerosol concentration, $M_{\rm tot.aerosol}~(\mu{\rm g}\cdot{\rm m}^{-3})$, is estimated based on

aerosol hygroscopicity. ω_{ox} is the mean molecular velocity (m-s⁻¹) of the oxidant and is calculated using eq 6 as follows⁴¹

$$\omega_{\rm ox} = \sqrt{\frac{8RT}{\pi MW}} \tag{6}$$

where MW is the molecular weight (kg·mol⁻¹). In our model, $f_{\rm abs,ox}$ was set at 4.2×10^{-6} in eq 5 to a have fast partitioning process. In general, partitioning is known to be a rapid process that can be completed within seconds. For example, Julin et al. eported that $\tau_{\rm GP,I}$ can be on the order of 10^{-10} s, which is much faster than gas-phase oxidation (order of 10^3-10^4 s) and aqueous-phase oxidation (order of 10^3-10^4 s). $k_{\rm des,ox}$ is determined using $k_{\rm abs,ox}$ and $K_{\rm p_ox}$ as follows

$$k_{\text{des,ox}} = \frac{k_{\text{abs,ox}}}{K_{\text{p,ox}}} \tag{7}$$

 $k_{
m des,ox}$ is sensitive to environmental conditions as it decreases when the humidity and organic matter in the algal aerosol increase

OH, radicals can also be produced via the photolysis of $\rm HONO^{45}$ and $\rm H_2O_2^{46}$ in the aerosol phase, as shown in eqs 8 and $\rm 9.^{36}$

$$\text{HONO}_{p} + h\nu \rightarrow \cdot \text{OH}_{p} + \text{NO} \quad j_{[\text{HONO}_{to}_{OH}]}$$
 (8)

$$H_2O_{2p} + h\nu \rightarrow 2 \cdot OH_p \quad j_{[HONO_to_OH]}$$
 (9)

Trace concentrations of $\rm H_2O_2$ and HONO are simulated from the photooxidation of hydrocarbons and $\rm NO_x$ using explicit gas mechanisms. The photolysis rate constants in the cyanobacterial algal aerosol are reduced by applying factor 0.1 to those in the gas phase. The photolysis rate of HONO in organic media such as cyanobacterial algae aerosol is unknown. The chromophores in an algal aerosol can absorb sunlight available for HONO photolysis and this can lessen the photolysis rates of HONO and $\rm H_2O_2$. In addition, HONO can undergo acid—base dissociation in aqueous solution and include other aqueous oxidation paths.

3.2. Oxidation of MC-LR in Algal Aerosol. The reaction rates of the ADDA moiety with O₃ and OH radicals are expressed in eqs 10 and 11, respectively.¹⁹

$$O_{3p} + MCLR_p$$
 $k_{MCLR,ozone}(s^{-1})$
 $\rightarrow O_{3}MCLR_p + 0.18 OH_p$ (10)

$$OH_p + MCLR_p \rightarrow OH_MCLR_p \quad k_{MCLR,OH}(s^{-1})$$
 (11)

 $k_{\rm MCLR,ozone}$ obtained by simulating ELISA data in the presence of O₃ in dark conditions was used to determine $k_{\rm MCLR,OH}$ under sunlight. eq 11 illustrates that the degradation of MC-LR via ozonolysis yields OH radicals. The OH radical is a biproduct produced from a Criegee biradical of an alkene ozonolysis product. The OH yield from ozonolysis of MC-LR or cyanobacterial algae aerosol is unidentified. The OH yield from ozonolysis of the dissolved organic matter in wastewater is reported as 0.13, and the average value of isoprene is 0.23. In this study, the OH yield of MC-LR was set to 0.18 (average value).

3.3. Integration of Chamber Data with the HAAR Model. As seen in Figure 1, major input variables for gas simulation include meteorological parameters (sunlight, temperature, and humidity) and the concentrations of

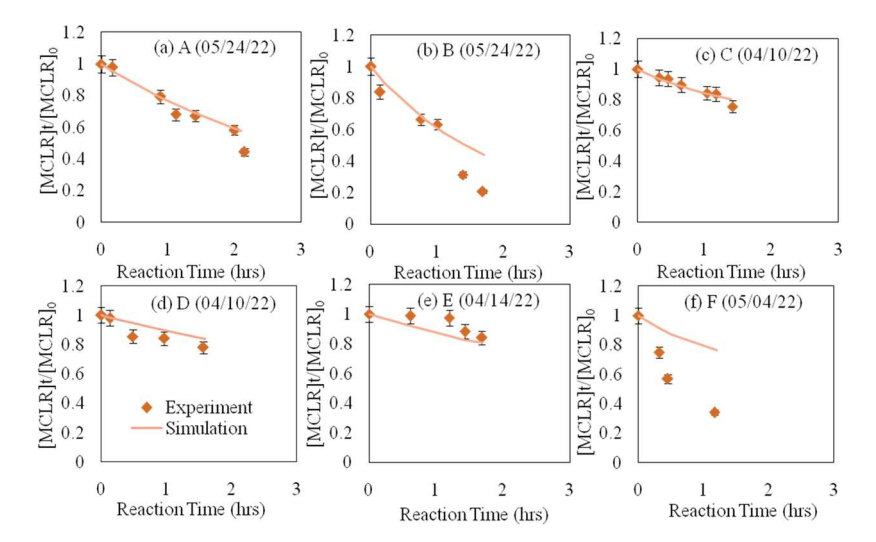


Figure 2. Degradation of MC-LR due to the reaction with ozone at nighttime (experiments A–F in Table 1). The error bars associated with ELISA were estimated with the standard error for the mean MC-LR concentration when $\alpha = 0.95$.

hydrocarbons (i.e., 2M2B and methane), NOx, and ozone (nighttime ozonolysis). The variables associated with algal aerosol include $M_{\rm or,dry}$ and $M_{\rm in,dry}$ to determine aerosol's hygroscopicity (Figure S3), and ultimately, they are used to estimate $V_{\mathrm{tot,aerosol}}$ (eq 1). The second-order reaction rate constant $(k_{\text{MCLR,ozone}})$ for the reaction of MC-LR with aerosolphase O₃ is determined via the HAAR simulation of the MCdecay by using nighttime ozonolysis chamber data (Section 4.2). In the presence of $k_{\text{MCLR,ozone}}$, the second-order reaction rate constant $(k_{MCLR,OH})$ for the reaction of MC-LR with OH radicals is determined by simulating daytime chamber data with the HAAR model (Section 4.3). For daytime simulation, atmospheric oxidants, such as OH radicals and ozone, are predicted via the simulation of the photooxidation of 2M2B in the presence of NO_x with the MCM gas mechanisms. The simulated oxidant concentrations are dynamically integrated with aqueous partitioning (Section 3.1) to heterogeneously oxidize MC-LR (Section 3.2). The processes in HAAR, including gas oxidation, multiphase partitioning, and MC-LR oxidation in algal aerosol, are performed under the DSMACC-KPP platform, as described in Section 2.1.

4. RESULTS AND DISCUSSION

4.1. Cyanobacterial Aerosol Composition. Figure S4 displays the FTIR spectra of organic matter in the cyanobacterial algae collected on the FTIR disk. As reported in the previous study by Jang et al., 19 MC-LR in both algal aerosols originating from M. aeruginosa and Anabaena sp. rapidly decayed. As seen in the FTIR spectra of Figure S4, the distributions of organic functional groups in both M. aeruginosa and Anabaena sp. cultures are almost similar. Thus, we assume that algal organic compositions that originate from different algal aerosols are similar and their impact on hygroscopicity and MC-LR decay can also be similar. The peak assignments for FTIR spectra are shown in Table S2. The FTIR spectrum was decoupled into functional groups using the curve fitting method, assuming that a Gaussian distribution governs each peak. The fitting parameters are the center frequency, the peak absorbance, and the half-width at half-height. 49 The relative functional group intensities for -OH (-NH), -COOH, C= O in ketones, C=O in amides, C-O, and C-N in amides were normalized with that of the C-H stretching. The

decoupled FTIR bend for each functional group was applied to estimate the functionality composition of algal aerosol using the relative intensity of the functional group determined from various reference compounds. The organic to carbon (O:C) ratio and the nitrogen to carbon (N:C) ratio were estimated with the resulting FTIR data to be 0.72 and 0.33, respectively, suggesting that cyanobacterial aerosol is highly hydrophilic. This aerosol functional group composition verifies our initial assumption of a single-homogeneous phase between organic and inorganic compositions under ambient humidity conditions.

A detailed description of the characterization of aerosol compositions of algal aerosol can be found in the chamber procedure of Section S1. In brief, an organic carbon (OC) analyzer (Sunset Laboratory) is used to identify $M_{\text{or,dry}}$ of the total cyanobacterial aerosol. Based on data from the Aerosol Chemical Speciation Monitor (ACSM, Aerodyne Research Inc., MA) and the data from ion chromatography, the predominant inorganic salts in both cases are sulfate (SO_4^{2-}) , sodium (Na^+) , potassium (K^+) , and nitrate (NO₃⁻), which originates from nitrogen-containing organic matter in cyanobacteria. In this study, the measurements of calcium, magnesium, and phosphate ions are, however, missing due to the limitation in an IC column and the method. May et al.13 reported in their field study that inorganic species were dominated by SO₄²⁻, Na⁺, potassium K⁺, and nitrate NO₃⁻. The measured $M_{\rm tot,dry}$ (SMPS data and aerosol density) well accords with the estimation obtained from $M_{\rm or,dry}$, $M_{\rm in,dry}$ (Table 1), and the aerosol water content (Section 2.2).

4.2. Ozonolysis of MC-LR. ELISA data in Figure 2 shows that the exposure of algal aerosol-containing MC-LR to O_3 alone causes significant decay to MC-LR concentrations, as the decrease between successive measurements exceeds the standard error of the preceding measurement. In all cases, O_3 is present at a stable concentration in the chamber in the presence of cyanobacterial aerosol, indicating that a pseudofirst-order reaction can approach MC-LR degradation. In the HAAR model simulation, $k_{\rm MCLR,ozone}$ determined for the reaction of MC-LR with aerosol-phase O_3 is 3×10^{-11} cc/molecules/s (Figure 1). The impact of humidity on MC-LR decay is clearly shown in Figure 2a,b (Exp. A at 36% and Exp. B at 95%, respectively). Under similar ozone concentrations

and chemical compositions, the decay of MC-LR is much faster in the higher RH. The high RH in Exp. B raises $V_{\text{tot,aerosol}}$ elevating the amount of ozone in algal aerosol (eq 1) as well as the rate of MC-LR decay. The O₃ concentration is significantly lower in Exp. C than in Exps. D and E, but RH in C (89%) is much higher than in the other two cases (Exps. D (49%) and E (43%)). As a result, there is no significant difference in the slopes of the decay curves of the three cases. The HAAR model well simulated MC-LR decay in all five experiments (Examples A-E) under different experimental conditions. The prediction of MC-LR decay is, however, underpredicted in Exp. F conducted with a high $M_{\text{or,dry}}/M_{\text{in,dry}}$ ratio under high RH. A possible explanation is that the current regression equation does not sufficiently predict the water content estimation in the organic portion for RH > 85%. When humidity exceeds 90%, the aerosol water content can be dramatically increased, even for the aerosol with high organics.

4.3. Degradation of Aerosolized MC-LR under Sunlight. The resulting ozonolysis rate constant of MC-LR in Section 4.2 was then applied to the daytime simulation to determine the reaction rate constant of MC-LR with the OH radical. The second-order reaction rate constant $(k_{MCLR,OH})$ for the reaction of MC-LR with OH radicals is 6×10^{-7} cc/molecules/s. Figure 3 shows that the simulated results with

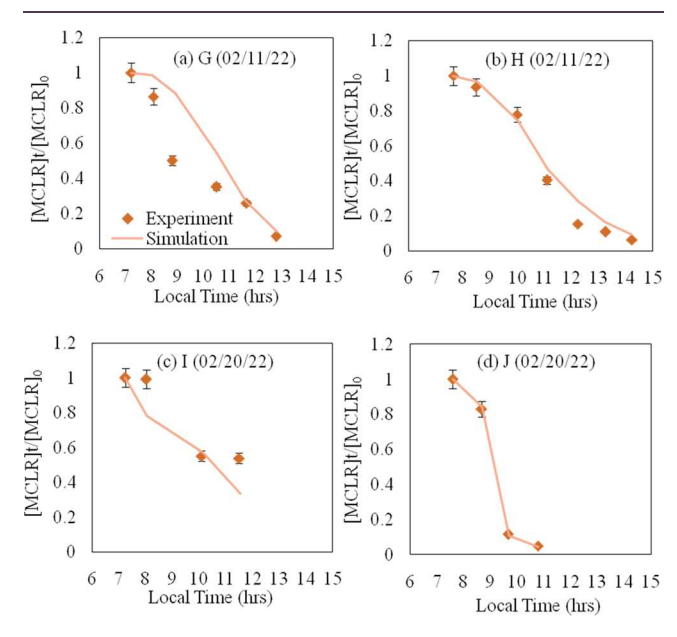


Figure 3. Degradation of MC-LR during daytime (experiments G–J in Table 1). The error bars associated with ELISA were estimated with the standard error for the mean MC-LR concentration when α = 0.95.

HAAR are in good agreement with experimental observations. In Figure 3a (Exp. G) and Figure 3b (Exp. H), the MC-LR decay was performed at two different NO_x levels (50 and 250 ppb). As seen in gas simulations in Figure S1, the NO_x level influences ozone formation, showing the lower ozone concentration under higher NO_x conditions. However, the impact of NO_x levels on MC-LR decay in algal aerosol is insignificant. Based on integrated reaction rate infrared reflectography (IRR), expressed as an accumulated chemical formation or consumption flux at a given reaction and initial concentration, the oxidation of MC-LR in the aerosol phase is primarily attributed to the reaction with the OH radical

generated mainly via photolysis of HONO. The OH radical partitioned from the gas phase can partly react with MC-LR, but it is minimal compared to that formed from HONO photolysis. The MC-LR decay under the low NO_x is attributed to ozone and the OH radical, while the OH radicals' reaction dominates under high NO_x conditions. For example, the IRR analysis shows that 80% of MC-LR in Exp. G (low NO_x) is oxidized by the OH radical and 98% of MC-LR in Exp. H (high NO_x).

In experiments I (Figure 3c) and J (Figure 3d), the MC-LR decay was examined for the case of low and high RH, respectively. Figure 3c (%RH = 25 on average) and Figure 3d (%RH = 81 on average) shows that higher RH conditions increase the degradation rate of MC-LR, although experimental conditions are somewhat different (Table 1). The details about the impact of the environmental conditions including RH, ozone, $M_{\rm or,dry}/M_{\rm in,dry}$, and temperature, are discussed in Section 5 below.

5. SENSITIVITY OF MC-LR DECAY TO ENVIRONMENTAL VARIABLES AND UNCERTAINTIES IN RATE CONSTANTS IN THE HAAR MODEL

The sensitivity of MC-LR decay to major variables under sunlight is illustrated in Figure 4: Temperature (Figure 4a, 283 vs 298 K), RH (Figure 4b, three RH levels at 20, 60, and 80%), $M_{\rm or,dry}/M_{\rm in,dry}$ (Figure 4c, three levels at 0.5, 1.0, and 2.0), and HC (ppbC)/NO_x(ppb) (Figure 4d, three levels at 3, 10, and 20). In Figure 4e, the sensitivity of the MC-LR ozonolysis to different ozone levels was examined in dark conditions. Among all of the environmental variables, humidity is the most influential on MC-LR decay, followed by $M_{\rm or,dry}/M_{\rm in,dry}$ ratios. On the other hand, the MC-LR decay is marginally influenced by temperature and NO_x levels. As standard conditions, the nighttime data from 04/10/22 were used to simulate all three cases ($[O_3]$ = 20, 50, 100 ppb). The results illustrated in Figure 4e show an increase by a factor of 2 and 5 times when the ozone concentration increases from 20 to 60 and 20 to 100 ppb, respectively. However, the oxidation of MC-LR by OH radicals dominates under sunlight; thus, the impact of ozone is less noteworthy, as discussed in Section 4.

Figure S5 illustrates the model uncertainties associated with the rate constant for predicting the decay of MC-LR under sunlight at given experimental conditions (02/20/2022, Table 1). The ELISA method employed to determine the concentration of MC-LR introduces an uncertainty in the reaction rate constants of MC-LR with ozone and OHradicals. Moreover, other factors, such as the calculation of the water content or Henry's law constants applied for the gasaerosol partitioning of the tracers, can introduce some uncertainty in the model. In order to estimate the uncertainty, the HAAR model runs under the same standard conditions increasing or decreasing the rate constant for both ozonolysis and reaction with OH by 50%. As seen in Figure S5, the decay of MC-LR by ozonolysis is much less critical during the daytime than that by the reaction with the OH radical. The OH radical is a powerful oxidant³⁶ with a rapid reaction rate with alkenes (i.e., an ADDA unit in MC-LR); thus, its reaction tends to occur on the surface when the diffusion of the OH radical in aerosol media or $k_{\rm abs,OH}$ is not extraordinarily fast. 50,51 In our study, MC-LR oxidation by the OH radical is limited by the absorption rate constant $(k_{abs,OH})$. As a result,

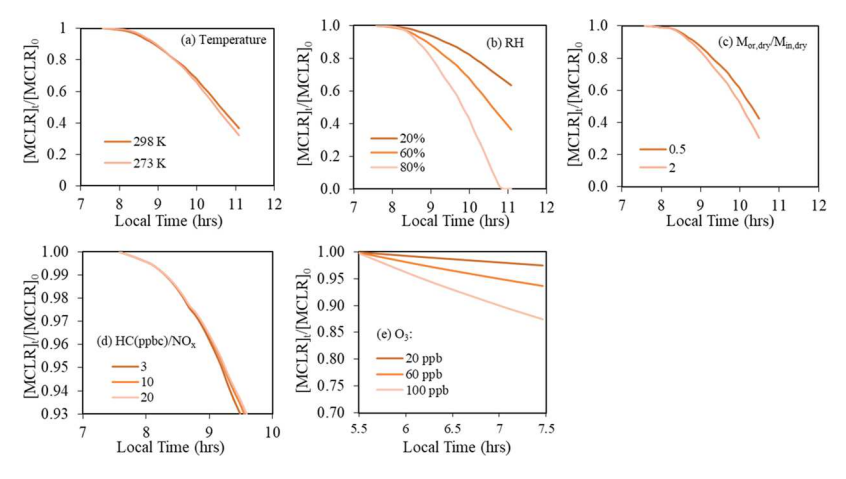


Figure 4. Sensitivity of MC-decay to environmental variables including temperature (a), humidity (b), $M_{\text{or,dry}}/M_{\text{in,dry}}$ (c), HC (ppbc)/NO_x (d), and ozone (e). For all of the simulations T = 298 K, RH = 60%, $M_{\text{or,dry}}/M_{\text{in,dry}} = 1$, HC (ppbc)/NO_x = 10, and the sunlight intensity measured on 02/20/2022 (Figure S7) are the standard selected conditions for the sensitivity analysis. For the ozone sensitivity test, the reference experimental conditions are taken from the data on 04/10/2022 (Table 1).

the MC-LR reaction with the OH radical stays unaffected by changes in $k_{\rm MCLR,OH}$ but is susceptible to $k_{\rm abs,OH}$. Unlike the diffuse-reactive parameter, q (Section 3.1), of the ozonolysis of MC-LR (order of 10^{-3}), that of the OH radical reaction ranges from 10^{-1} to 10^{0} , suggesting that the reaction potential on the aerosol surface is higher.

6. ATMOSPHERIC IMPLICATIONS

The HAAR model of this study was developed to predict the oxidation of MC-LR by O₃ and OH using comprehensive kinetic mechanisms in the aerosol phase. The hygroscopicity of cyanobacterial algal aerosol and its chemical composition was incorporated into the model to estimate the overall impact of humidity and the content of both organic and inorganic constituents on MC-LR decay. The HAAR model simulates experimentally observed outdoor chamber data (Figures 2 and 3) in both nighttime and daytime conditions. The model simulation results suggest that the gas-aerosol partitioning of oxidants increases with increasing humidity due to the increased aerosol mass and the $M_{\text{or,dry}}/M_{\text{in,dry}}$ ratio in algal aerosol owing to increased solubility of oxidants (eq 1). As discussed in the uncertainty analysis, the MC-LR degradation is mainly attributed to its reaction with the OH radical under sunlight. The ozonolysis of MC-LR is important at nighttime, although less noteworthy than that with the OH radical during daytime. The HAAR model suggests that the MC-LR decay is significantly sensitive to humidity changes and relatively less sensitive to $M_{\rm or,dry}/M_{\rm in,dry}$ ratios or temperature changes. In our study, the MC-LR decay with the photooxidation of 2M2B was unaffected by changes in NO_x levels. In addition to gas-phase OH radicals, the HONO produced at high NO_x levels can be dissolved in aqueous algal aerosol and heterogeneously form OH radicals that can react with MC-LR. In the future, the sensitivity of the MC-LR decay to NO, levels needs to be evaluated with urban hydrocarbons (i.e., gasoline). In our study, the temperature dependence of rate constants, $k_{\text{MCLR,ozone}}$ and $k_{\text{MCLR,OH}}$, was not considered. Both Anabaena sp. culture and M. aeruginosa culture of this study showed similarity in organic compositions (Figure S4). However, numerous types of cyanobacteria are involved in the production of algal aerosols during harmful algae blooms.

Thus, further characterization for algal aerosol compositions generated from various algae cultures is needed.

Under sunlight near the summer solstice at Gainesville, Florida, the half-life of degradation of MC-LR, which is introduced to the ambient air at 11 AM with 20 ppb 2-methyl-2-butene, 30 ppb NO_x, 18 ppb formaldehyde, and 6ppb acetaldehyde at 298 K and 70% RH, is simulated by using the HAAR model. The estimated half-life during the daytime is about 6 minutes. At nighttime, the estimated lifetime of MC-LR in the presence of 66 ppb ozone (Exp. C in Table 1) is 4.6 h. Thus, the degradation of MC-LR is dominated by the reaction with OH radicals under ambient sunlight. When airborne MCs are fluxed in the middle of the day (maximum sunlight), their lifetime can be even shorter than 6 minutes with increased HONO and H₂O₂ concentrations.

During the summer, the average wind speed in the largest lake (i.e., Okeechobee) in Florida is 5.7 mph (9.2 km/h).52 For a 6-min half-life of the MC-LR, the air can horizontally travel 0.92 km from the bloom. In applying a Gaussian dispersion model to predict the transport of aerosolized cyanobacterial MCs from algal bloom events, the dispersion can be assumed to occur mainly in the vertical direction due to the formation of aerosol from a line source.⁵³ During moderate sunlight conditions, 75% of aerosolized MC-LR undergoes dispersion within approximately 0.92 km from the bloom, suggesting that the atmospheric process (25% of MC-LR concentration) significantly contributes to the decay of aerosolized MC-LR. For the MC-LR emitted from blooms to the atmosphere under the maximum sunlight (half-life < 6min), the influence of atmospheric oxidation on MC-LR might be much greater than 25%. MCs emitting from cyanobacterial algae blooms can influence the residence and recreation areas near lakes and estuaries although the concentration of airborne MCs decreases via the dispersion and photochemical oxidation processes during transportation. However, the exposure levels of airborne MCs are still unclear and not well established. Most exposure guidelines for aerosolized MCs are based on the water level cell counts and MC concentrations. For example, the estimated exposure of air concentrations of MCs was in the level of pg·m⁻³ above a lake with the water concentration of MCs higher than 5 orders of magnitude in Microcystis sp. (cells·mL⁻¹) of up to 3 orders of

magnitude in total MCs μ g·L^{-1.54} Studies suggest that inhaled MCs can affect pulmonary health, and they are likely to accumulate in the liver with longer-term exposure. The reactive oxygen species (ROS) can also be produced during the atmospheric process of the cyanobacterial aerosol and its toxins. The significance of airborne ROS on pulmonary health during algae breaks needs to be investigated.

In this study, the reaction of MC-LR with nitrate radicals was not considered. Although the nitrate radical (NO₃) reaction with hydrocarbons is not significant during the daytime due to its photolysis, NO3 is generally important during the nighttime. The vital source of NO3 is the decomposition of N₂O₅ via a thermodynamic equilibrium reaction to form NO2 and NO3. In the presence of aqueous aerosol, N2O5 reacts with water forming HNO3, which significantly reduces the concentration of NO₃.⁵⁷ Therefore, the contribution of NO₃ might be insignificant for the MC-LR decay in ambient air. The sulfur species, including SO₂, H₂S₃ and dimethyl sulfide, are emitted from anthropogenic fuel combustions and wetlands and produce sulfuric acid via homogeneous gas-phase reactions and heterogeneous aqueous reactions in the aerosol phase. The role of aerosol acidity associated with sulfuric acid also needs to be studied in future research.

In addition to MC-LR, there is a wide variety of MCs in cyanobacterial algae. Thus, the HAAR model needs to be extended to other MCs to simulate the atmospheric processes of algal toxins. However, major MCs, including MC-LR, MC-RR, MC-YR, and MC-WR, generally comprise the unique ADDA unit that can be highly reactive to atmospheric oxidants dissolved in the aqueous algal aerosol. Thus, the HAAR model of this study can be suitable for simulating the degradation of other MCs as well. Although atmospheric oxidants can rapidly oxidize the ADDA units that are the focal points for algal toxicity in the daytime, the toxicity of cyanobacterial algal aerosol is still poorly studied and need to be investigated in the future.

ASSOCIATED CONTENT

Supporting Information

The Supporting Information is available free of charge at https://pubs.acs.org/doi/10.1021/acsearthspace-chem.3c00050.

Gas simulation of the photooxidation of 2-methyl-2-butene (2M2B) in the presence of NO_x under ambient sunlight (Figure S1); total UV irradiation during the chamber experiment conducted on 02/20/2022 (Figure S2); HAAR model parameters (Table S1); hygroscopicity properties of inorganic and organic constituents of the fresh cyanobacterial algal aerosol (Figure S3); FTIR spectrum and its peak assignments of organic constituents in cyanobacterial algal aerosol (Figure S4 and Table S2); and uncertainties of the simulated degradation of MC-LR in cyanobacteria algal aerosol using the HAAR model (Figure S5) (PDF)

■ AUTHOR INFORMATION

Corresponding Author

Myoseon Jang — Department of Environmental Engineering Sciences, University of Florida, Gainesville, Florida 32611, United States; ⊚ orcid.org/0000-0003-4211-7883; Phone: +1-352-846-1744; Email: mjang@ufl.edu

Authors

Victoria Zorbas – Department of Environmental Engineering Sciences, University of Florida, Gainesville, Florida 32611, United States

Baharan Emam — Department of Environmental Engineering Sciences, University of Florida, Gainesville, Florida 32611, United States; Department of Environmental Health Engineering, School of Public Health and Safety, Shahid Beheshti University of Medical Sciences, Tehran 198353-5511. Iran

Jiwon Choi – Department of Environmental Engineering Sciences, University of Florida, Gainesville, Florida 32611, United States

Complete contact information is available at: https://pubs.acs.org/10.1021/acsearthspacechem.3c00050

Author Contributions

The manuscript was written through the contributions of all authors. All authors have given approval to the final version of the manuscript.

Notes

The authors declare no competing financial interest.

ACKNOWLEDGMENTS

This work was supported by grants from the National Science Foundation (AGS1923651 and CBET 2044921) and the Florida Fish and Wildlife Conservation Commission (PO # B9B593).

REFERENCES

- (1) Wells, M. L.; Trainer, V. L.; Smayda, T. J.; Karlson, B. S. O.; Trick, C. G.; Kudela, R. M.; Ishikawa, A.; Bernard, S.; Wulff, A.; Anderson, D. M.; Cochlan, W. P. Harmful algal blooms and climate change: Learning from the past and present to forecast the future. *Harmful Algae* 2015, 49, 68–93.
- (2) Mbukwa, E. A.; Msagati, T. A. M.; Mamba, B. B. Quantitative Variations of Intracellular Microcystin-LR, -RR and -YR in Samples Collected from Four Locations in Hartbeespoort Dam in North West Province (South Africa) During the 2010/2011 Summer Season. *Int. J. Environ. Res. Public Health* 2012, *9*, 3484–3505.
- (3) Carmichael, W. W.; Falconer, I. R.Diseases Related to Freshwater Blue-Green Algal Toxins, and Control Measures. In Algal Toxins in Seafood and Drinking Water; Academic Press, 1993 https://www.google.com/url?sa=t&rct=j&q=&esrc=s&source=web&cd=&cad=rja&uact=8&ved=2ahUKEwjS8o_S1Kf8AhXdRPEDHXb3DssQFnoECAkQAQ&url=https%3A%2F%2Fagris.fao.org%2Fagrissearch%2Fsearch.do%3FrecordID%3DGB9416832&usg=AOvVaw2bQ4LVzaeD5sTBsBKU64sjpp187-209.
- (4) Carmichael, W. W.; Azevedo, S. M.; An, J. S.; Molica, R. J.; Jochimsen, E. M.; Lau, S.; Rinehart, K. L.; Shaw, G. R.; Eaglesham, G. K. Human fatalities from cyanobacteria: chemical and biological evidence for cyanotoxins. *Environ. Health Perspect.* **2001**, *109*, 663–668.
- (5) Kirkpatrick, B.; Fleming, L. E.; Squicciarini, D.; Backer, L. C.; Clark, R.; Abraham, W.; Benson, J.; Cheng, Y. S.; Johnson, D.; Pierce, R.; et al. Literature Review of Florida Red Tide: Implications for Human Health Effects. *Harmful Algae* **2004**, *3*, 99–115.
- (6) Moore, S. K.; Trainer, V. L.; Mantua, N. J.; Parker, M. S.; Laws, E. A.; Backer, L. C.; Fleming, L. E. Impacts of climate variability and future climate change on harmful algal blooms and human health. *Environmental Health* **2008**, *7*, No. S4.
- (7) Grattan, L. M.; Holobaugh, S.; Morris, J. G. Harmful algal blooms and public health. *Harmful Algae* **2016**, *57*, 2–8.

- (8) Seegers, B. N.; Werdell, P. J.; Vandermeulen, R. A.; Salls, W.; Stumpf, R. P.; Schaeffer, B. A.; Owens, T. J.; Bailey, S. W.; Scott, J. P.; Loftin, K. A. Satellites for long-term monitoring of inland U.S. lakes: The MERIS time series and application for chlorophyll-a. *Remote Sens. Environ.* 2021, 266, 112685. DOI: DOI: 10.1016/j.rse.2021.112685 https://www.sciencedirect.com/science/article/pii/S0034425721004053.
- (9) Vesterkvist, P. S. M.; Misiorek, J. O.; Spoof, L. E. M.; Toivola, D. M.; Meriluoto, J. A. O. Comparative Cellular Toxicity of Hydrophilic and Hydrophobic Microcystins on Caco-2 Cells. *Toxins* **2012**, *4*, 1008–1023.
- (10) Young, F. M.; Metcalf, J. S.; Meriluoto, J. A. O.; Spoof, L.; Morrison, L. F.; Codd, G. A. Production of antibodies against microcystin-RR for the assessment of purified microcystins and cyanobacterial environmental samples. *Toxicon* **2006**, *48*, 295–306.
- (11) Wang, C.; Gu, S.; Yin, X.; Yuan, M.; Xiang, Z.; Li, Z.; Cao, H.; Meng, X.; Hu, K.; Han, X. The toxic effects of microcystin-LR on mouse lungs and alveolar type II epithelial cells. *Toxicon* **2016**, *115*, 81–88.
- (12) Axson, J. L.; May, N. W.; Colón-Bernal, I. D.; Pratt, K. A.; Ault, A. P. Lake Spray Aerosol: A Chemical Signature from Individual Ambient Particles. *Environ. Sci. Technol.* **2016**, *50*, 9835–9845.
- (13) May, N. W.; Olson, N. E.; Panas, M.; Axson, J. L.; Tirella, P. S.; Kirpes, R. M.; Craig, R. L.; Gunsch, M. J.; China, S.; Laskin, A.; et al. Aerosol Emissions from Great Lakes Harmful Algal Blooms. *Environ. Sci. Technol.* **2018**, *52*, 397–405.
- (14) Plaas, H. E.; Paerl, H. W. Toxic Cyanobacteria: A Growing Threat to Water and Air Quality. *Environ. Sci. Technol.* **2021**, *55*, 44–64
- (15) Olson, N. E.; Cooke, M. E.; Shi, J. H.; Birbeck, J. A.; Westrick, J. A.; Ault, A. P. Harmful Algal Bloom Toxins in Aerosol Generated from Inland Lake Water. *Environ. Sci. Technol.* **2020**, *54*, 4769–4780.
- (16) Hu, J.; Liu, J.; Zhu, Y.; Diaz-Perez, Z.; Sheridan, M.; Royer, H.; Leibensperger, R.; Maizel, D.; Brand, L.; Popendorf, K. J.; et al. Exposure to Aerosolized Algal Toxins in South Florida Increases Short- and Long-Term Health Risk in Drosophila Model of Aging. *Toxins* **2020**, *12*, No. 787.
- (17) Heisler, J.; Glibert, P. M.; Burkholder, J. M.; Anderson, D. M.; Cochlan, W.; Dennison, W. C.; Dortch, Q.; Gobler, C. J.; Heil, C. A.; Humphries, E.; et al. Eutrophication and harmful algal blooms: A scientific consensus. *Harmful Algae* **2008**, *8*, 3–13.
- (18) Song, W.; Bardowell, S.; O'Shea, K. E. Mechanistic Study and the Influence of Oxygen on the Photosensitized Transformations of Microcystins (Cyanotoxins). *Environ. Sci. Technol.* **2007**, *41*, 5336–5341.
- (19) Jang, M.; Berthold, D. E.; Yu, Z.; Silva-Sanchez, C.; Laughinghouse Iv, H. D.; Denslow, N. D.; Han, S. Atmospheric Progression of Microcystin-LR from Cyanobacterial Aerosols. *Environ. Sci. Technol. Lett.* **2020**, *7*, 740–745.
- (20) Laughinghouse, H. D.; Prá, D.; Silva-Stenico, M. E.; Rieger, A.; Frescura, V. D.-S.; Fiore, M. F.; Tedesco, S. B. Biomonitoring genotoxicity and cytotoxicity of Microcystis aeruginosa (Chroococcales, Cyanobacteria) using the Allium cepa test. *Sci. Total Environ.* **2012**, 432, 180–188.
- (21) Werner, V. R.; Laughinghouse Iv, H. D. Bloom-forming and other planktonic Anabaena (Cyanobacteria) morphospecies with twisted trichomes from Rio Grande do Sul State, Brazil. *Nova Hedwigia* **2009**, *89*, 17.
- (22) Lefler Forrest, W.; Barbosa, M.; Berthold David, E.; Laughinghouse, H. D. Genome Sequences of Two Microcystis aeruginosa (Chroococcales, Cyanobacteria) Strains from Florida (United States) with Disparate Toxigenic Potentials. *Microbiol. Resour. Announce.* 2020, 9, e00844–00820 (accessed 2023/04/07).10.1128/MRA.00844-20 (accessed 2023/04/07).
- (23) Orsini, D. A.; Ma, Y.; Sullivan, A.; Sierau, B.; Baumann, K.; Weber, R. J. Refinements to the particle-into-liquid sampler (PILS) for ground and airborne measurements of water soluble aerosol composition. *Atmos. Environ.* **2003**, *37*, 1243–1259.

- (24) Jiang, H.; Jang, M. Dynamic Oxidative Potential of Atmospheric Organic Aerosol under Ambient Sunlight. *Environ. Sci. Technol.* **2018**, *52*, 7496–7504.
- (25) Jiang, H.; Jang, M.; Sabo-Attwood, T.; Robinson, S. E. Oxidative potential of secondary organic aerosols produced from photooxidation of different hydrocarbons using outdoor chamber under ambient sunlight. *Atmos. Environ.* **2016**, *131*, 382–389.
- (26) Li, J.; Jang, M. Aerosol Acidity Measurement Using Colorimetry Coupled With a Reflectance UV-Visible Spectrometer. *Aerosol Sci. Technol.* **2012**, *46*, 833–842.
- (27) Jang, J.; Jang, M.; Mui, W.; Delcomyn, C. A.; Henley, M. V.; Hearn, J. D. Formation of Active Chlorine Oxidants in Saline-Oxone Aerosol. *Aerosol Sci. Technol.* **2010**, *44*, 1018–1026.
- (28) Beardsley, R.; Jang, M.; Ori, B.; Im, Y.; Delcomyn, C. A.; Witherspoon, N. Role of sea salt aerosols in the formation of aromatic secondary organic aerosol: yields and hygroscopic properties. *Environ. Chem.* **2013**, *10*, 167–177.
- (29) Zhong, M.; Jang, M. Dynamic light absorption of biomass-burning organic carbon photochemically aged under natural sunlight. *Atmos. Chem. Phys.* **2014**, *14*, 1517–1525.
- (30) Nenes, A.; Pandis, S. N.; Pilinis, C. ISORROPIA: A New Thermodynamic Equilibrium Model for Multiphase Multicomponent Inorganic Aerosols. *Aquat. Geochem.* **1998**, *4*, 123–152.
- (31) Clegg, S. L.; Brimblecombe, P.; Wexler, A. S. Thermodynamic Model of the System H+-NH4+-SO42--NO3--H2O at Tropospheric Temperatures. *J. Phys. Chem. A* **1998**, *102*, 2137-2154.
- (32) Emmerson, K. M.; Evans, M. J. Comparison of tropospheric gas-phase chemistry schemes for use within global models. *Atmos. Chem. Phys.* **2009**, *9*, 1831–1845.
- (33) Damian, V.; Sandu, A.; Damian, M.; Potra, F.; Carmichael, G. R. The kinetic preprocessor KPP-a software environment for solving chemical kinetics. *Comput. Chem. Eng.* **2002**, *26*, 1567–1579.
- (34) University of York; Wolfson Foundation, U. o. Y. National Centre for Atmospheric Science Wolfson Atmospheric Chemistry Laboratories, 2013 http://mcm.york.ac.uk/.https://www.york.ac.uk/chemistry/research/wacl/.
- (35) Hanson, D. R.; Ravishankara, A. R.; Solomon, S. Heterogeneous reactions in sulfuric acid aerosols: A framework for model calculations. *J. Geophys. Res.: Atmos.* **1994**, *99*, 3615–3629 acccessed 2023/04/08.
- (36) Finlayson-Pitts, B. J. P.; J, N., Jr Chemistry of the Upper and Lower Atmosphere. Academic Press 2000. https://www.elsevier.com/books/chemistry-of-the-upper-and-lower-atmosphere/finlayson-pitts/978-0-12-257060-5.
- (37) Chameides, W. L. Compilation of Henry's law constants (version 4.0) for water as solvent, *Atmos. Chem. Phys.*, **1984**, *89*, 4739–4755. https://henrys-law.org/henry/notes.html.
- (38) Sander, R. Compilation of Henry's law constants (version 4.0) for water as solvent. *Atmos. Chem. Phys.* **2015**, *15*, 4399–4981.
- (39) Biń, A. K. Ozone Solubility in Liquids. *Ozone: Sci. Eng.* **2006**, 28, 67–75.
- (40) Kamens, R.; Jang, M.; Chien, C.-J.; Leach, K. Aerosol Formation from the Reaction of α -Pinene and Ozone Using a Gas-Phase Kinetics-Aerosol Partitioning Model. *Environ. Sci. Technol.* **1999**, 33, 1430–1438.
- (41) Yu, Z.; Jang, M.; Kim, S.; Son, K.; Han, S.; Madhu, A.; Park, J. Secondary organic aerosol formation via multiphase reaction of hydrocarbons in urban atmospheres using CAMx integrated with the UNIPAR model. *Atmos. Chem. Phys.* **2022**, 22, 9083–9098.
- (42) Han, S.; Jang, M. Simulating the impact of gas-wall partitioning on SOA formation using the explicit gas mechanism integrated with aqueous reactions containing electrolytes. *Sci. Total Environ.* **2020**, 748, No. 141360. From NLM From NLM
- (43) Yu, Z.; Jang, M.; Park, J. Modeling atmospheric mineral aerosol chemistry to predict heterogeneous photooxidation of SO2. *Atmos. Chem. Phys.* **2017**, *17*, 10001–10017.
- (44) Julin, J.; Winkler, P. M.; Donahue, N. M.; Wagner, P. E.; Riipinen, I. Near-Unity Mass Accommodation Coefficient of Organic

Molecules of Varying Structure. Environ. Sci. Technol. 2014, 48, 12083-12089.

- (45) Bongartz, A.; Kames, J.; Schurath, U.; George, C.; Mirabel, P.; Ponche, J. L. Experimental determination of HONO mass accommodation coefficients using two different techniques. *J. Atmos. Chem.* **1994**, *18*, 149–169.
- (46) Goldstein, S.; Aschengrau, D.; Diamant, Y.; Rabani, J. Photolysis of Aqueous H2O2: Quantum Yield and Applications for Polychromatic UV Actinometry in Photoreactors. *Environ. Sci. Technol.* **2007**, *41*, 7486–7490.
- (47) Liang, J.; Jacobson, M. Z. A study of sulfur dioxide oxidation oxidation pathways over a range of liquid water contents, pH values, and temperatures. *J. Geophys. Res.: Atmos.* **1999**, *104*, 13749–13770.
- (48) Nöthe, T.; Fahlenkamp, H.; Sonntag, Cv. Ozonation of Wastewater: Rate of Ozone Consumption and Hydroxyl Radical Yield. *Environ. Sci. Technol.* **2009**, *43*, 5990–5995.
- (49) Jang, M.; Kamens, R. M. Characterization of Secondary Aerosol from the Photooxidation of Toluene in the Presence of NOx and 1-Propene. *Environ. Sci. Technol.* **2001**, *35*, 3626–3639.
- (50) Li, J.; Jang, M.; Beardsley, R. L. Dialkylsulfate formation in sulfuric acid-seeded secondary organic aerosol produced using an outdoor chamber under natural sunlight. *Environ. Chem.* **2016**, *13*, 590–601.
- (51) Yu, Z.; Jang, M.; Zhang, T.; Madhu, A.; Han, S. Simulation of Monoterpene SOA Formation by Multiphase Reactions Using Explicit Mechanisms. ACS Earth Space Chem. 2021, 5, 1455–1467.
- (52) Spark, W. weatherspark.com/y/18765/Average-. https://weatherspark.com/y/18765/Average-Weather-in-Okeechobee-Florida-United-States-Year-Round.
- (53) Turner, D. B. Workbook of Atmospheric Dispersion Estimates: An Introduction to Dispersion Modeling; CRC Press, 2020 DOI: 10.1201/9780138733704.
- (54) Wood, S. A.; Dietrich, D. R. Quantitative assessment of aerosolized cyanobacterial toxins at two New Zealand lakes. *J. Environ. Monit.* **2011**, *13*, 1617–1624.
- (55) Breidenbach, J. D.; French, B. W.; Gordon, T. T.; Kleinhenz, A. L.; Khalaf, F. K.; Willey, J. C.; Hammersley, J. R.; Mark Wooten, R.; Crawford, E. L.; Modyanov, N. N.; et al. Microcystin-LR aerosol induces inflammatory responses in healthy human primary airway epithelium. *Environ. Int.* **2022**, *169*, No. 107531.
- (56) Organization, W. H. Cyanobacterial toxins: microcystins. Background document for development of WHO Guidelines for drinking-water quality and Guidelines for safe recreational water environments *Geneva:*. *Licence: CC BY-NCSA 3.0 IGO 2020* https://www.who.int/publications/m/item/background-documents-for-development-of-who-guidelines-for-drinking-water-quality-and-guidelines-for-safe-recreational-water-environments.
- (57) Han, S. J. M. Modeling Diurnal Variation of SOA Formation via Multiphase Reactions of Biogenic Hydrocarbons. *Atmos. Chem. Phys. Discussions* **2022**, 1–25.

□ Recommended by ACS

Photoenhanced Radical Formation in Aqueous Mixtures of Levoglucosan and Benzoquinone: Implications to Photochemical Aging of Biomass-Burning Organic Aerosols

Lena Gerritz, Manabu Shiraiwa, et al.

JUNE 07, 2023

THE JOURNAL OF PHYSICAL CHEMISTRY A

READ 🗹

Molecular Tracer Characterization during COVID-19 Pandemic in Shanghai: Changes in the Aerosol Aqueous Environment and Implications for Secondary Organic Ae...

Fan Fan, Qingyan Fu, et al.

DECEMBER 06, 2022

ACS EARTH AND SPACE CHEMISTRY

READ 🗹

Growth Rate Dependence of Secondary Organic Aerosol on Seed Particle Size, Composition, and Phase

Devon N. Higgins, Murray V. Johnston, et al.

AUGUST 10, 2022

ACS EARTH AND SPACE CHEMISTRY

READ 🗹

Differences in Photosensitized Release of VOCs from Illuminated Seawater versus Freshwater Surfaces

Laura T. Stirchak, D. James Donaldson, et al.

AUGUST 31, 2021

ACS EARTH AND SPACE CHEMISTRY

READ 🗹

Get More Suggestions >